ELSEVIER

Journal of Molecular Catalysis A: Chemical 161 (2000) 105–113

JOURNAL OF MOLECULAR CATALYSIS A: CHEMICAL

www.elsevier.com/locate/molcata

Cerium dioxide as a photocatalyst for water decomposition to O_2 in the presence of Ce^{4+}_{aq} and Fe^{3+}_{aq} species

Gratian R. Bamwenda*, Hironori Arakawa

National Institute of Materials, and Chemical Research, 1-1 Higashi, Tsukuba, Ibaraki, 305-8565 Japan

Received 19 February 2000; accepted 8 May 2000

Abstract

It has been demonstrated that cerium dioxide is a potential photocatalyst that can be used to decompose water to produce oxygen in aqueous suspension containing an electron acceptor, and the optimum parameters for the reaction have been investigated. The O_2 yield strongly depended on the duration of irradiation, CeO_2 concentration, concentration of the electron acceptor, and pH of the suspension. The optimum photoproduction for O_2 was obtained under the following operating conditions: Illumination time: >10 h, CeO_2 concentration: 2–5 g dm^{-3}, $[Ce^{4+}]$: 4–5 mM, pH <3, and illumination wavelength <420 nm. During long-term runs, CeO_2 suspensions showed a satisfactory photostability and activity even after 400 h of illumination. The obtained data show that, with an appropriate design, cerium dioxide is a promising material that can be used as a photoactive component in photocatalytic reactions. The studied system utilizes CeO_2 to accomplish the initial light absorption, charge separation, and O_2 evolution from the interaction of water molecules with holes photogenerated in the CeO_2 valence band, in the presence of Ce^{4+}_{aq} or Fe^{3+}_{aq} species as an acceptor of conduction band electrons.

Keywords: Ceria; Photocatalysts; Ceric and ferric cations; Water oxidation; Oxygen

1. Introduction

Photocatalytic reactions using metal oxide semiconductor powders have been paid much attention because of the possible practical application of such systems for water decomposition to hydrogen and oxygen, and in a wide range of chemical redox reactions such as the mineralization of organic pollutants in waste water [1–7].

Recently, interest in the photooxidation of water over oxide semiconductor electrodes and suspensions has been growing steadily because such systems can be used in the production of oxygen, and in the clean up technology of water polluted with inorganic and organic pollutants. In our previous reports [5,6], we have described the production of oxygen and hydrogen from aqueous tungsten oxide suspensions and we have been searching for other materials that can be used in such reactions.

The purpose of this work has been to investigate the performance of CeO_2 as a material for photoassisted water splitting to produce oxygen, and to determine the optimum reaction conditions for the reaction. The choice of CeO_2 was prompted by the fact that among the metal oxides we have tested so

* Corresponding author. Tel.: +81-298-54-4760; fax: +81-298-54-4750.

1381-1169/00/$ - see front matter
PII: S1381-1169(00)00270-3

Table 1
Selected physicochemical properties of cerium oxide

Property	Value	Literature
Color	yellowish-white	this work
Density	7.1 g cm^{-3}	[8]
Surface area	~9.5 m^2 g^{-1}	this work
Acidity	weak base	this work
ΔH^0_{f298}	−246 kcal mol^{-1}	[8]
$T_{melting}$	2873 K	[8]
Crystal system	face-centered cubic	[8]
Electronegativity	2.3 pauling	[9]
Absorption edge	~420 nm	this work
Bandgap[a]	~2.95 eV	this work
Conductivity	$1.2–2\times10^{-8}$ Ω^{-1} cm^{-1}	[10]

[a]The bandgap was estimated from the plot of the UV–VIS absorption vs. λ and using the equation: $E_{BG} = 1240/\lambda_{onset}$.

far, CeO_2 has interesting economical and physicochemical properties. Cerium dioxide is abundant, nontoxic and inexpensive. Furthermore, CeO_2 is a semiconducting material that absorbs light in the near UV and slightly in the visible region. These features make cerium dioxide a promising material that can be used in heterogeneous photocatalytic reactions. Other selected properties of cerium dioxide are given in Table 1.

On the other hand, cerium has +1, +3 and +4 oxidation states. These oxidation states make cerium cations to be an attractive species as an electron acceptor or sacrificial agent in aqueous photoelectrochemical reactions since they can oxidize and reduce reversibly ($E^0_{Ce^{3+}/Ce^{4+}} = +1.44$ V). Despite the fact that Ce^{3+}/Ce^{4+} is a simple redox couple, its use in photocatalytic reactions has not been widely explored. In this work, we use the transfer of an electron from the photoexcited CeO_2 particle to surface-adsorbed Ce^{4+}_{aq} as way of improving the e^-–h^+ charge separation and the subsequent migration of the charges to active centers on the CeO_2 surface, where the decomposition of adsorbed water molecules takes place.

2. Experimental

2.1. Materials

High purity powdered CeO_2 (99.9% purity) was obtained from Wako Chemical. The surface area of the powder measured by nitrogen adsorption was ~9.5 m^2 g^{-1}. Cerium sulfate (99.5%, Wako Chemical) was used as supplied. Solutions of Ce^{4+} and Fe^{3+} were made by dissolving $Ce(SO_4)_2 \cdot nH_2O$ and $Fe_2(SO_4)_3 \cdot nH_2O$ ($n = 3–4$, Kokusan Chemical) in distilled, deionized water. Other materials such as NaOH and H_2SO_4 acid (Wako Chemical) were of analytical grade and were used as supplied.

2.2. Apparatus and procedures

CeO_2 (0.4–1.6 g) was dispersed in 90 cm^3 of distilled, deionized water and required amounts of electron acceptors such as Ce^{4+} and Fe^{3+} aqueous solutions were added so that the final volume was about 100 and 350 cm^3 for the outer- and inner-irradiation photoreactors, respectively. The suspension was then transferred to the reactor and then the reactor was mounted to a closed gas-circulation system (~215 cm^{-3}), equipped with outlets to a vacuum line and GC.

Experiments were performed in two types of reactors: Outer-irradiation type photoreactor; i.e. a Pyrex cell having a 23-cm^2 flat window for illumination with a capacity of ~215 cm^3. In this case, the irradiation of the suspension was carried out from the outside of the reactor by a 500-W xenon lamp (Ushio UXL 500D) with an incident flux of 500 mW cm^{-2}, as measured with an Eppley Lab. radiometer. The second cell is an annular (inner-irradiation type) photoreactor, in which irradiation from a 400-W high pressure mercury lamp (Riko Kagaku) is transverse. In this setup, light is transmitted through a Pyrex or quartz glass water jacket, which is immersed vertically in a 1.1-dm^3 Pyrex glass cylinder ($\phi = 75$ mm) containing a 350 cm^3 dispersion.

Prior to illumination, the mixture was evacuated up to ~2 kPa under magnetic stirring to remove physisorbed gases. After a 2 h deaeration, that is when almost no O_2 was detected by on-line GC, small amounts of argon were added to the system and the experiment was started by illuminating the suspension, under continuous stirring, at an initial pressure of between 4 and 7 kPa. The course of the reaction was monitored by periodic sampling of the gas phase. The average reaction temperature was 300 and 311 ± 3 K for the inner- and outer-irradiation systems, respectively.

2.3. Analyses

The diffuse reflectance UV–VIS spectra of the powders, in the absorbance mode, were recorded on a Shimadzu MPS-2000 spectrometer between 700 and 200 nm. The optical band gap E_g was calculated based on the absorbance spectrum of the powders, using Eq. (1).

$$E_{BG} = 1240/\lambda_{Absorp.\,Edge} \quad (1)$$

BET surface areas were measured by nitrogen adsorption at liquid nitrogen temperature using a Gemini 2360 surface area analyzer.

X-ray diffraction patterns were recorded between $2\theta = 10–80^0$ using a Mac Science diffractometer with CuKα radiation.

Oxygen and hydrogen were analyzed by gas chromatography (Shimadzu GC-8A) equipped with a thermal conductivity detector (TCD) and a stainless steel column (2 m) packed with molecular sieves 5 A at 318 K. Argon was used as a carrier gas. Several reproducibility tests were performed over a range of various irradiation times. The uncertainty in the measurement of H_2 and O_2 yields was found to be less than 5% in the majority of experiments, which was adequate for the purpose of the present investigation.

3. Results

3.1. Characterization

The XRD patterns of the initial and used CeO_2 powders are shown in Fig. 1. The only discernible peaks were those due to cerianite with cubic structure [11]. As can be seen in Fig. 1, no readily noticeable corrosion or photoetching were noticed in the X-ray diffraction patterns of CeO_2 even after 20 h of irradiation in the form of an aqueous suspension.

Fig. 2 shows the absorption spectra acquired for CeO_2 powders before (Fig. 2a) and after the reaction (Fig. 2b). The spectra in Fig. 2 show that CeO_2 has an intense absorption in the UV that trails into the visible region of the spectrum. The onset of absorption of CeO_2 was at $\sim$420 nm, which corresponds to the bandgap energy of ca. 2.95 eV. This value is consistent with the characteristic values given in literature for CeO_2 materials, i.e. ($E_{BGCeO_2} = 2.8–3.2$ eV) [12,13]. A slight red shift of the absorption onset of the powders and an increase of absorbance in the visible and red region were noticed after the reaction.

Fig. 3 depicts the spectra of aqueous solutions of $Ce(SO_4)_2$ (Fig. 3a) and that of the supernatant after

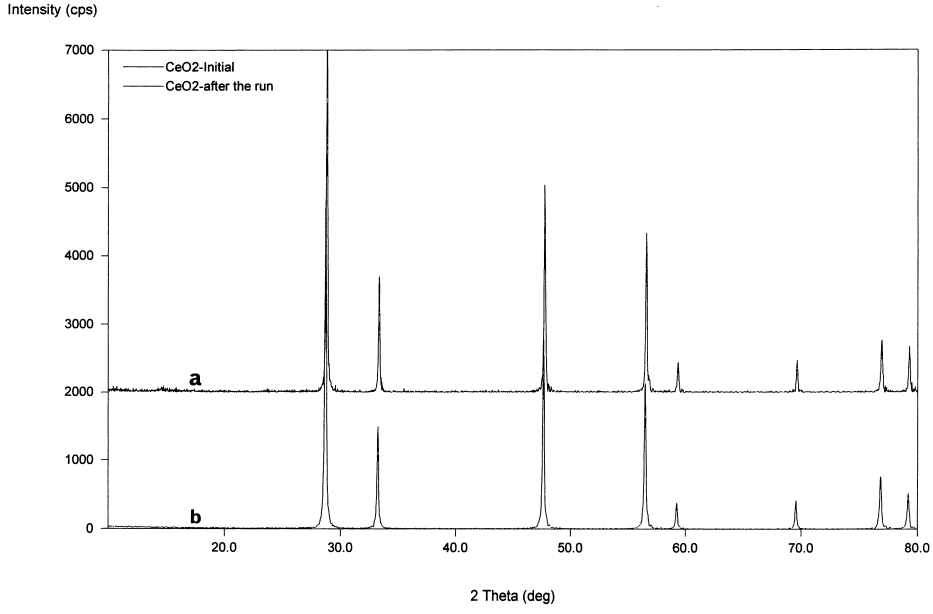

Fig. 1. X-ray diffraction patterns of cerium dioxide before (a), and after reaction (b).

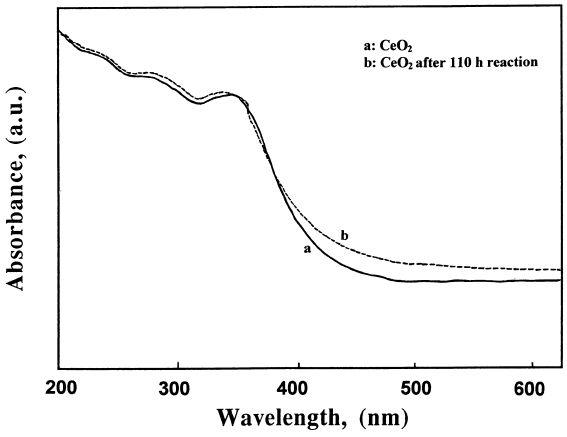

Fig. 2. UV–VIS diffuse reflectance spectra of cerium dioxide before (a), and after reaction (b).

the reaction (Fig. 3b). As seen in Fig. 3, Ce^{4+}_{aq} solutions strongly absorb in the UV region and weakly absorb in the visible region. The absorption edge of supernatant ceric sulfate solutions shifted in the blue region with illumination time and its absorption coefficient decreased as the reaction progressed. The results reported in Fig. 3b lead us to suppose that in Ce^{4+} dilute aqueous solutions, $[Ce^{4+}] \leq 5$ mM, the solution phase will not significantly interfere with the absorption by CeO_2 particles.

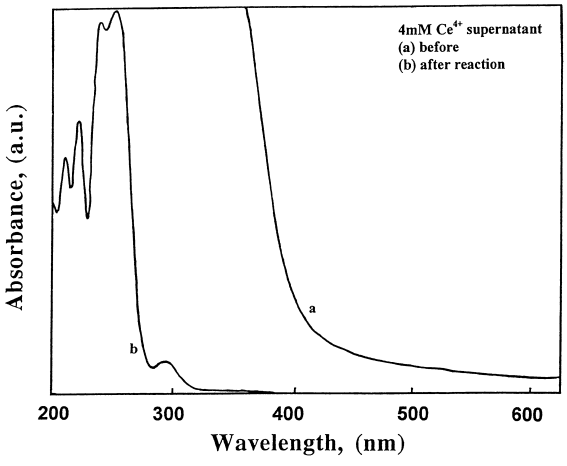

Fig. 3. UV–VIS diffuse reflectance spectra of the initial cerium sulfate solution (a), and that of the supernatant after a 24 h-illumination.

3.2. Photocatalytic production of oxygen

3.2.1. Dependence of O_2 yield on illumination time and concentration of CeO_2

In blank runs without light, no O_2 was detected from 10 mM Ce^{4+}_{aq} solutions alone or in the presence of CeO_2 in a 50-h strong agitation (800 rpm). No O_2 was detected from a 30-h irradiation of the $Ce(SO_4)_2$ solution alone; only 0.07 μmol H_2 evolved. This indicates that so as to efficiently oxidize water to produce O_2, the system must contain CeO_2, which under illumination generates and separates charges, offer energetic holes and surface sites for water oxidation.

By irradiating an aqueous suspension containing CeO_2 and Ce^{4+}_{aq} species, an evolution of O_2 was observed. The variation of the O_2 yield as a function of illumination time and on CeO_2 concentration in the suspension dispersed in an annular reactor is displayed in Fig. 4. After an initial induction period of 0.5–1 h, the yield of O_2 increased with illumination time reaching ca. 300 μmol after 10 h of irradiation for suspension containing 4.6 g CeO_2 dm^{-3} and 4 mM Ce^{4+}_{aq}. In addition, the O_2 yield increased in proportion to the CeO_2 content in the suspension, and leveled off at $C_{CeO_2} > 5$ g dm^{-3}. Although not shown, runs were also performed using

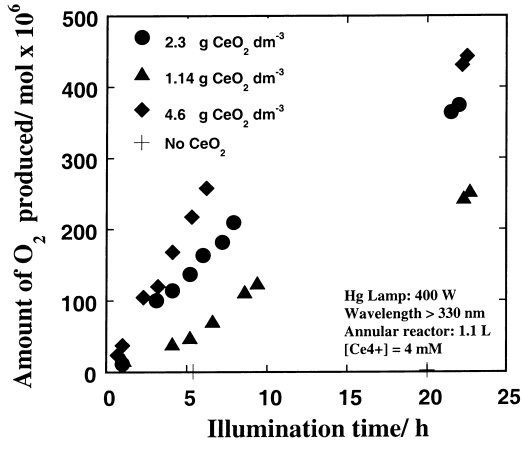

Fig. 4. Time course of oxygen evolution as a function of illumination time and concentration of CeO_2 in the suspension. Conditions: 1.1 dm^{-3} annular reactor; suspension: 0.35 dm^{-3}; 400 W Hg lamp; $\lambda_i \geq 300$ nm; electron acceptor: 4 mM Ce^{4+}, $T = 311 \pm 3$ K, mixing with magnetic stirrer at a speed: 850 rpm.

appropriate light filters to examine the influence of illumination wavelength range on the O_2 evolution activity. It was found that only the light with wavelength below 400 nm was efficient for both CeO_2 bandgap photoexcitation and the evolution of O_2. Under illumination with light of wavelengths $\lambda_i \geq 300$ nm, oxygen evolution was about two orders of magnitude than in the case of $\lambda_i \geq 420$ nm, indicating that visible and red wavelength lines are beyond the energy barrier for CeO_2.

3.2.2. Dependence on the concentration of Ce^{4+}_{aq}

The amount of O_2 produced was found to be dependent on the initial concentration of Ce^{4+}_{aq} species in the suspension. The plots of the amount of O_2 evolved vs. concentration of Ce^{4+} are shown in Fig. 5. The O_2 yield increased in proportion to Ce^{4+}_{aq} concentration passing through a maximum at 4–5 mmol Ce^{4+} dm^{-3}. It is worth mentioning here that the color of the Ce^{4+}_{aq} solution changed from almost colorless at low concentrations to yellow with increasing concentration of Ce^{4+}_{aq}. Definitely an increase in the Ce^{4+}_{aq} concentration led to an increase in the inner filter effect by the solution.

3.2.3. pH dependence

The pH dependence on the reaction was also investigated and the O_2 production as a function of pH is plotted in Fig. 6. As seen, the amount of O_2 evolved was strongly dependent upon the initial pH.

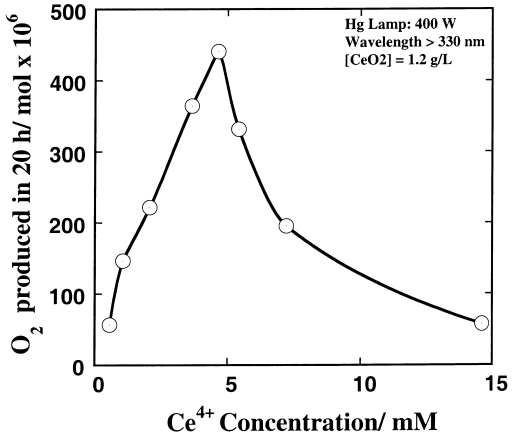

Fig. 5. Influence of Ce^{4+} concentration on the yield of O_2. Other conditions as in Fig. 4.

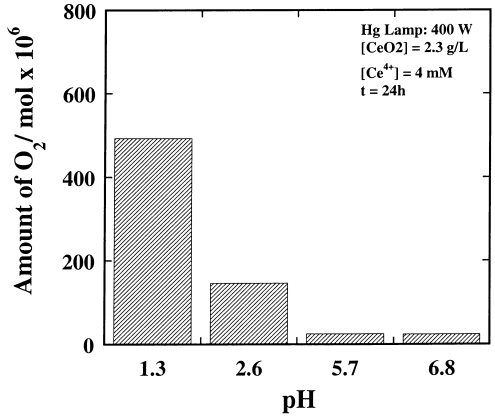

Fig. 6. Dependence of O_2 yield on the pH of the dispersion. Irradiation time: 20 h; $[CeO_2] = 2.3$ g/L, $[Ce^{4+}] = 1.1$ mol dm^{-3}.

The pH values below pH 3 gave better O_2 yields, whereas increase in pH resulted in a considerable decrease in the O_2 yield. One of the significant result is the feasibility of producing O_2 in suspensions with pH > 6. Most of the active electron acceptors used previously had a tendency of forming light absorbing precipitates at pH > 4 [6].

3.2.4. Comparison of Ce^{4+} and Fe^{3+} as electron acceptors

During irradiation runs with CeO_2 suspended in distilled, deionized water in the absence of the electron acceptor only trace amounts of H_2 or O_2 (0.5–3 μmol) were produced, as shown in Fig. 7. As previously mentioned, addition of small amounts of an electron acceptor to the suspension resulted in the enhancement of the evolution of oxygen. Fig 7 compares the production of O_2 from CeO_2 aqueous suspensions containing Ce^{4+}_{aq}, and Fe^{3+}_{aq} species, which we have previously shown to be satisfactory electron acceptors in other systems [6]. Similar trends in O_2 production behavior were observed for both electron acceptors. The initial rates were comparable for both systems but in the case of suspension containing Ce^{4+}_{aq} species the yield leveled off faster than in the suspension containing Fe^{3+}_{aq}. The greater long-term yields observed for experiments with Fe^{3+}_{aq} than with Ce^{4+}_{aq} may possibly be due to the differences in the adsorbability of Ce^{4+}_{aq}, and Fe^{3+}_{aq} to hydrated CeO_2 particles and/or the ability of the formed

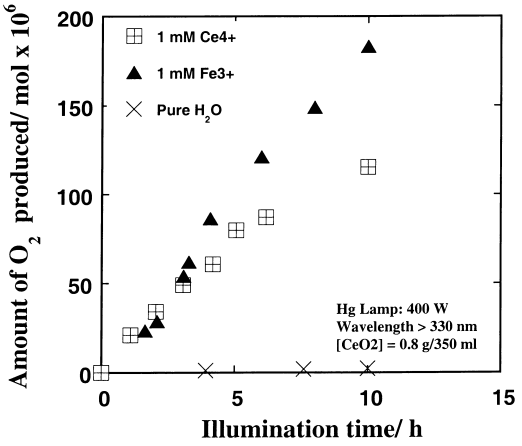

Fig. 7. The activity of CeO_2 for O_2 evolution from suspensions containing Ce^{4+}_{aq} and Fe^{3+}_{aq} as electron acceptors.

Fe^{2+}_{aq} ions to easily migrate away from the particle into the solution, thereby preventing the back reaction.

3.2.5. Long-term stability

To explore the long-term stability of the system, the activity of CeO_2 was examined in the presence of Fe^{3+}_{aq} species by series of runs that were conducted for more than 100 h followed by evacuating the system and re-irradiation after changing the supernatant. For this purpose, a 220-cm^3 outer-irradiation reactor with a 500-W Xe lamp were used so as to facilitate the ease of evacuating and changing solutions. The O_2 evolution profiles from such an outer-irradiation system are illustrated in Fig. 8. Illumination of the suspension resulted in the production of O_2 and small amounts of H_2 in proportion to the irradiation time, followed by a gradual decrease in the production rate at longer illumination periods (cycle I). Three possible causes for this decrease in rate were postulated; namely deactivation of CeO_2 or pressure buildup in the gas phase and/or the depletion of the electron acceptor species, Fe^{3+}_{aq}. To determine the cause of the decline in rates, after 100 h of irradiation the system was evacuated and the suspension was flushed with argon to remove the accumulated gases and the suspension was reirradiated. It is apparent in cycle II that the yield of O_2 dropped drastically whereas that of H_2 was unchanged. In cycle III, the CeO_2 was filtered, washed four times, and dispersed again in a fresh Fe^{3+} solution and reirradiated. The initial activity of CeO_2 was restored almost to that in the first cycle although the production of O_2 reached a plateau after $\sim$150 h of illumination. These results indicate that the observed decrease in production rates with time can be mainly attributed to the conversion of Fe^{3+}_{aq} into Fe^{2+}_{aq} ions as the reaction progresses, i.e. the depletion of the electron acceptor and, as consequence increasing the probability of the deleterious electron-hole recombination. This, in turn, will eventually lead to the fall of the rate of water decomposition to O_2. Based on the above findings, we deduce that the investigated system exhibits a consistent long-term activity toward O_2 production that may last even a couple of days.

3.2.6. Comparison with other materials

A comparison of the performance of CeO_2 powders with those of other materials is presented in Table 2. Cerium dioxide faired well when compared with other examined semiconducting oxides. CeO_2 powders prepared by air calcination of inorganic precursors showed better activity than the commercial samples. CeO_2 prepared from $CeCl_3$ gave the best O_2 yields. Among other oxides, TiO_2-P25 exhibited the highest activity. The differences in performance between materials illustrated in Table 2 may stem from possible differences in purity, concentration of defects in the materials, the level of crystallinity, photoelectronic properties, charge mobility and in the rate of electron injection from the

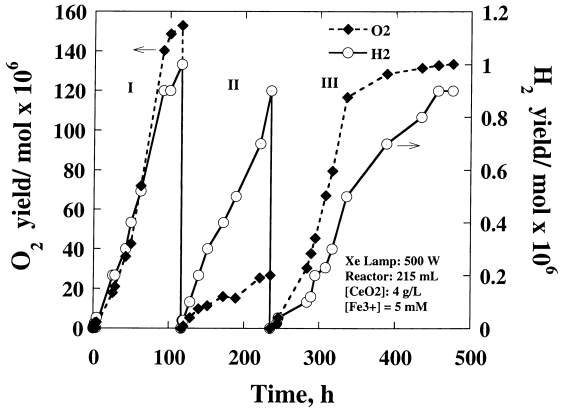

Fig. 8. The long-term activity of the CeO_2 aqueous suspension.

Table 2
The properties and activity of CeO_2 powders in comparison with other materials

Precursor		Sample	S_{BET} ($m^2\ g^{-1}$)	E_g (eV)[a]	r_{O_2} ($\mu mol\ h^{-1}$)
1	–	Cu_2O	5	2.21	< 0.1
2	–	Fe_2O_3	8	2.20	1.7
3	–	ZnO	30	3.17	8.1
4	–	CeO_2	9	2.95	18.5
5	$Ce_2(SO_4)_3 \cdot 8H_2O$	CeO_2	2	2.94	29.9
6	$CeCl_3 \cdot 7H_2O$	CeO_2	50	2.88	66.8
7	$Ce(NO_3)_3 \cdot 6H_2O$	CeO_2	61	2.97	37.1
8	$(NH_4)_6W_{12}O_{39}$	WO_3	3	2.49	56.3
9	–	TiO_2-P25	49	2.98	326.4
10	$Nb(OH)_5$	Nb_2O_5	55	3.50	17.5

The precursors were air annealed at between 723 and 1073 K for 4–7 h. Commercial powders Cu_2O (99.9%), Fe_2O_3 (99.9%) and ZnO (99.9%) were obtained from Wako Chemical. TiO_2-P25 was obtained from Degussa.
Reaction conditions: Annular reactor: 1.1 dm^3; 0.35 dm^3 suspension; C_{CeO_2}: 1.14 g dm^{-3}, pH = 2.5–3, light source: 400 Hg lamp; T: ~ 303 K, mixing with magnetic stirrer at a speed: 850 rpm.
[a] λ_{AE} and E_g — are the absorption onset and optical band gap, respectively. They were estimated from the UV–VIS absorbance spectra of the powders taken at room temperature. E_g was estimated by using the equation, $E_g = 1240/\lambda_{AE}$.

photoexcited metal oxide particle to the 4f orbital of Ce^{4+}_{aq}. A further study is under way to examine the effect of these parameters on the photocatalytic activity of CeO_2.

4. Discussion

4.1. Effect of reaction parameters on O_2 production

The present study has established several basic features concerning the performance of CeO_2 as a photocatalyst for the decomposition of water. The following is an attempt to rationalize the results presented in the preceding section.

From the data displayed in Figs. 4–8 and Table 2, it can be seen that CeO_2 exhibits a satisfactory activity and a good photostability, but the rate of O_2 evolution decreases with prolonged illumination. The fall in the O_2 production rate with time can be ascribed to the gradual transformation of Ce^{4+}_{aq} into Ce^{3+}_{aq}, and Fe^{3+}_{aq} into Fe^{2+}_{aq} and the subsequent depletion of the electron acceptor in the vicinity of CeO_2 particles as the reaction progresses. The lack of fast adequate replenishment of Ce^{4+}_{aq} and Fe^{3+}_{aq} ions will negatively affect the rate of interaction between these cations and the photogenerated electrons and, as a consequence, it will increase the probability of the deleterious electron-hole recombination. This, in turn, will eventually lead to the fall of the rate of water oxidation to O_2. Other possible reasons may be the loss of part of the photogenerated holes in the reverse reaction involving the oxidation of Ce^{3+}_{aq}, and Fe^{2+}_{aq} back to Ce^{4+}_{aq} and Fe^{3+}_{aq}. In addition, some of the photoproduced and dissolved oxygen may be consumed in a slow oxidation of Fe^{2+}_{aq} and Ce^{3+}_{aq} process that takes place in oxygen-rich aqueous acidic solutions [14].

As to the effect of pH, as anticipated, the evolution of O_2 decreased with the increase in pH. This is in agreement with the observation of Weber et al. [15a] and Bratermann et al. [15b] that the surface activity of associated cations to scavenge the photogenerated electrons shifts in the unfavorable direction with increase in pH. Furthermore, at pH > 4 the amount of electron acceptors is reduced to negligible amounts due to the precipitation of Fe^{3+} ions into a red-brown, light absorbing $Fe(OH)_3$ ($pK_s = 37.4$), and the conversion of cerous ions into yellow $CeOH^{3+}$ and $Ce(OH)^{2+}_2$. Other possible reasons include the shift of flatband potential of CeO_2 particles and redox potentials of the electron acceptor with pH, and the variation of the charging process of the surface of CeO_2 particles with pH.

The activity enhancement observed with increasing Ce^{4+}_{aq} concentration in the examined range may be partly explained by the fact that a gradual rise in

Ce^{4+}_{aq} concentration will lead to higher interfacial concentrations of electron acceptor species. This will subsequently result in the increased access of a large population of Ce^{4+}_{aq} ions in the vicinity of the CeO_2 particle surface. This, in turn, increases the probability of interaction between photogenerated electrons and Ce^{4+} species, thus improving the overall electron-hole pair dissociation and charge separation, thus favoring the reaction of photogenerated holes with adsorbed water molecules and the oxygen evolution process. Also, a sufficiently large population of Ce^{4+} species in the proximity of a CeO_2 particulate may create a suitable electric field, which can lead to Ce^{4+}_{aq} cations to act as surfaces states that can trap photogenerated electrons. This may help the e^-–h^+ charge separation.

The results from this study indicate that there are several competitive properties that affect the activity of the CeO_2–H_2O–Ce^{4+}_{aq}–$h\nu$ system during the photodecomposition of water. In order to obtain an optimum photocatalytic activity and product yields, a precise control is indispensable to satisfy most of the reaction parameters and the crucial properties of cerium dioxide and the suspension. Chemical modification of the cerium dioxide surface is underway so as to catalyze charge transfer across the cerium dioxide–water interface, and to improve and optimize the efficiency of water decomposition to O_2 and eventually water splitting to both oxygen and hydrogen in a two-step photocatalytic–photoredox process.

4.2. Mechanism

The following mechanism is proposed for the observed production of O_2. The reaction is initiated when light energy larger than the band-gap of a cerium dioxide is absorbed by the particles forming an electron (e^-) and hole (h^+) pair in CeO_2 as described in Eq. (2). The deleterious recombination of photogenerated electrons and holes in the lattice Eq (3) can be avoided if the two species are separated and subsequently trapped by appropriate sites on the particle surface defects or transferred to species bound to the surface, as illustrated in Eqs. (4) and (5).

Light absorption and charge generation:

$$(CeO_2) + h\nu \rightarrow e^-_{CB} + h^+_{VB} \quad (2)$$

$$e^-_{CB} + h^+_{VB} \rightarrow \text{recombination} \rightarrow \text{heat} \quad (3)$$

$$e^-_{CB} \rightarrow e^-_{tr} \quad (4)$$

$$h^+_{VB} \rightarrow h^+_{tr} \quad (5)$$

The subscript CB and VB denote conduction and valence bands, respectively.

Following photoexcitation and trapping of charges, surface-adsorbed Ce^{4+} or Fe^{3+} scavenges away the trapped electrons at the interface forming its reduced state Ce^{3+} or Fe^{2+} according to reactions (6) and (7) [16,17].

Reduction reaction:

$$e^-_{tr} + Fe^{3+}_{aq} \rightarrow Fe^{2+}_{aq} \quad (6)$$

$$e^-_{tr} + Ce^{4+}_{aq} \rightarrow Ce^{3+}_{aq}. \quad (7)$$

In this case, the role of the Fe^{3+} and Ce^{4+} is the removal of electrons from electron-hole recombination sites with the production of their lower oxidation states. It should be mentioned that it is also possible that other adsorbed ions on the particle surface, e.g. OH^- may produce an electric field, which promotes charge separation [18].

Simultaneously, the trapped holes in reaction (5) oxidize adsorbed water molecules in a four-electron exchange process, with a consequent evolution of gaseous oxygen as expressed in reaction (8).

Decomposition of water and oxygen formation:

$$4h^+_{tr} + 2H_2O \rightarrow 4H^+_{aq} + O_{2(gas)}. \quad (8)$$

As the concentration of O_2 and Ce^{3+}_{aq} or Fe^{2+}_{aq} cations increases, there remains the possibility that other secondary pathways may take place: (a) The reduction of produced but still adsorbed oxygen by e^-_{tr} to generate O^-_2 or equivalent species and (b) the interaction of h^+_{tr} with Ce^{3+}_{aq} or Fe^{2+}_{aq} regenerating Ce^{4+}_{aq} and Fe^{3+}_{aq}.

Other processes:

$$O_{2(ads)} + e_{tr}^- \rightarrow O_{2(ads)}^- \quad (9)$$

$$O_{2(ads)}^- + H^+ \xrightarrow{e_{tr}^-} HO_2 \xrightarrow{e_{tr}^-} HO_2^- \xrightarrow{H^+} H_2O_2 \quad (10)$$

$$OH^- + h_{tr} \rightarrow OH\cdot \quad (11)$$

$$Fe_{aq}^{2+} + h_{tr}^+ \rightarrow Fe_{aq}^{3+} \quad (12)$$

$$Ce_{aq}^{3+} + h_{tr}^+ \rightarrow Ce_{aq}^{4+} \quad (13)$$

Such side reactions as in Eqs.(9)–(11) would eventually negatively affect the rate of O_2 production. For example, $O_{2(ads)}^-$ can react with protons generated from reaction (8) to form $HO_2\cdot$ and subsequent products as shown in Eqs. (10) and (11).

On the other hand, reverse processes such as those in reactions (12) and (13) can have a positive effect by replenishing Ce_{aq}^{3+} or Fe_{aq}^{2+} species necessary for reactions (6) and (7).

The series of reactions (2)–(8) lead to the formation of O_2 according to the following overall reaction:

$$4Me_{aq}^{n+} + 2H_2O \xrightarrow[CeO_2]{h\nu} 4Me_{aq}^{(n-1)+} + 4H^+ + O_{2(gas)}\cdot \quad (14)$$

5. Conclusion

The present study has established several basic features concerning the performance of CeO_2 as a photocatalyst for the decomposition of water. The obtained results demonstrate that aqueous CeO_2 suspensions containing Ce_{aq}^{4+} and Fe_{aq}^{3+} are stable and active toward O_2 production and small amounts of H_2 under a variety of operating conditions. The production of O_2 was found to be sensitive to illumination time, concentration of CeO_2, initial concentration of the electron acceptor and pH. The present data show that, with an appropriate design, cerium dioxide is a promising material that can be used as a photoactive component for the photoproduction of O_2. Detailed studies of this system are in progress and attempts are being made to use cerium dioxide as a photocatalyst for overall water splitting to oxygen and hydrogen and the results from such systems will be published in a subsequent paper of this series.

References

[1] J. Yoshimura, Y. Ebina, A. Tanaka, J. Kondo, K. Domen, J. Phys. Chem. 97 (1993) 1970.
[2] S. Tabata, H. Nishida, K. Tabata, Catal. Lett. 34 (1995) 245.
[3] K.H. Chung, D.C. Park, Catal. Today 30 (1996) 157.
[4] T. Ohno, D. Haga, K. Fujihara, K. Kaizaki, M. Matsumura, J. Phys. Chem. B 101 (1997) 6415.
[5] K. Sayama, R. Yoshida, H. Kusama, K. Okabe, Y. Abe, H. Arakawa, Chem. Phys. Lett. 277 (1997) 387.
[6] G.R. Bamwenda, K. Sayama, H. Arakawa, J. Photochem. Photobiol., A,Chem 122 (1999) 175.
[7] N. Serpone, E. Pelizzetti, H. Hidaka, in: D.F. Ollis, H. Al-Ekabi (Eds.), Photocatalytic Purification and Treatment of Water and Air, Elsevier, London, 1993, p. 225.
[8] K.A. Gscheidner, L. Eyring (Eds.), Handbook on the Physics and Chemistry of the Rare Earths vol. 8 North Holland, Amsterdam, 1986, p. 139.
[9] R.J. Sanderson, J. Am. Chem. Soc. 74 (1952) 272.
[10] S. Bernal, J.J. Calvino, G.A. Cifredo, A. Laachir, V. Perrichon, J.M. Hermann, Langmuir 10 (1994) 717.
[11] JCPDS Card No. 43-1002.
[12] C.A. Hogath, Z.T. Al-Dhhan, Phys. Status Solidi B 137 (1986) K157.
[13] K.B. Sundaram, P. Wahid, Phys. Status Solidi B 161 (1990) K64.
[14] T. Tzedakis, A. Savall, M.J. Clifton, J. Appl. Electrochem. 19 (1989) 911.
[15a] J. Weber, Z. Samec, V. Marecek, J. Electroanal. Chem. 89 (1978) 271.
[15b] P.S. Bratermann, A.G. Cairns-Smith, R.W. Sloper, T.G. Truscott, M.J. Craw, J. Chem. Soc., Dalton Trans. 7 (1984) 1441, and references therein.
[16] A.A. Kranovskii, G.P. Brin, Dokl. Akad. Nauk SSSR 147 (1962) 656.
[17] J. Weiss, Nature 136 (1935) 794.
[18] A.L. Linseberger, G. Lu, J.T. Yates, Chem. Rev. (Washington, D. C.) 95 (1995) 735.